Common regulatory mutation increases single-cell survival to antibiotic exposures in *Pseudomonas aeruginosa*.

David Ritz[1], Yijie Deng[2], Daniel Schultz[1]*

[1] Department of Microbiology & Immunology, Geisel School of Medicine, [2] Thayer School of Engineering – Dartmouth College, Hanover, NH 03755, USA.

* Correspondence:

Daniel.Schultz@dartmouth.edu

Abstract

Typical antibiotic susceptibility testing (AST) of microbial samples is performed in homogeneous cultures in steady environments, which does not account for the highly heterogeneous and dynamic nature of antibiotic responses. The most common mutation found in *P. aeruginosa* lineages evolved in the human lung, a loss of function of repressor MexZ, increases basal levels of multidrug efflux MexXY, but does not increase resistance by traditional MIC measures. Here, we use single cell microfluidics to show that *P. aeruginosa* response to aminoglycosides is highly heterogeneous, with only a subpopulation of cells surviving exposure. *mexZ* mutations then bypass the lengthy process of MexXY activation, increasing survival to sudden drug exposures and conferring a fitness advantage in fluctuating environments. We propose a simple “Response Dynamics” assay to quantify the speed of population-level recovery to drug exposures. This assay can be used alongside MIC for resistance profiling to better predict clinical outcomes.

Introduction

The human host presents a complex and dynamic environment for the evolution of opportunistic pathogens. While establishing infections, such microbes encounter various new challenges, including antibiotic treatments where they are periodically exposed to much larger doses of antibiotics than what is found in nature[1]. Opportunistic pathogens are typically equipped with a variety of inducible mechanisms of antibiotic resistance, but sudden exposures require quick responses, while gene expression is still possible[2,3]. Consequently, not all cells are able to successfully mount a response to antibiotic challenges, which often leads to the coexistence of live and dead (or arrested) cells[4]. This heterogeneity influences treatment outcomes and complicates the antibiotic susceptibility testing (AST) of pathogens[5]. Still, susceptibility profiling of pathogens in the lab typically only estimates the minimum inhibitory concentration (MIC) of antibiotics in bulk bacterial cultures, which does not account for the noisy dynamics of drug responses.

P. aeruginosa, an opportunistic bacterial pathogen, is a leading cause of infections in human hosts. It is particularly associated with cystic fibrosis (CF), a genetic disease that causes mucus buildup in the lung, which becomes prone to colonization by bacteria, resulting in loss of lung function[6,7]. *P. aeruginosa* infections are typically acquired from unique environmental clone types naïve to the human host[8], but lineages evolved in chronic infections eventually diversify into heterogeneous populations with remarkably altered phenotypes, including reduced virulence, transition to biofilm growth and antibiotic resistance[9–12]. Antibiotics, particularly aminoglycosides, have been routinely used to treat *P. aeruginosa* infections[13]. Although early infections can sometimes be cleared[14], chronic infections are difficult to eradicate[15] even with high doses of antibiotics. Therefore, a maintenance therapy of multiple courses of administration is usually needed to control the bacterial load in the airways[1], which has been shown to increase the incidence of resistance to the applied antibiotics[16]. However, the selective pressures driving this increase in antibiotic resistance in *P. aeruginosa* in the CF lung are not well understood.

While environmental *P. aeruginosa* strains can use a variety of resistance mechanisms[17], virtually all aminoglycoside-resistant strains found in the CF lung show some degree of upregulation of the multi-drug resistance *mexXY* operon (**Fig 1A**)[18,19], which codes for an inner-membrane antiporter MexY and a periplasmic fusion protein MexX[20] that mediate the export of a variety of different drugs, including most aminoglycosides[21]. Induction of the aminoglycoside response is primarily regulated by MexZ, a transcription repressor of *mexXY*[22,23]. In strains with a wild type *mexZ* allele, the activation of *mexXY* is caused by a decrease in translation efficiency, and not from a direct interaction with the drugs themselves, which allows resistance to be activated by a wide variety of stressors[24,25]. The outcome of drug treatments therefore depends on a lengthy process of MexXY activation that spans up to ~6 hours, which only starts when translation is already compromised[26].

Recent studies found that the single most common mutation observed in CF clinical

samples is the loss of function of MexZ[27,28], resulting in upregulation and higher basal levels of *mexXY* expression[29]. Despite being common in clinical samples, the evolution of *mexZ* mutants has not yet been reproduced in vitro in standard serial passage experiments[30,31], and *mexZ* mutations do not appear to significantly increase the MIC of aminoglycosides[32]. However, these studies assessed resistance under steady drug concentrations, where MexXY is fully induced in wild type and *mexZ* mutants alike[29]. Therefore, we investigate the possibility that such regulatory mutations are beneficial during induction of the response, before full expression is reached. We utilize single-cell and population-level assays to test the hypothesis that the continuous expression of *mexXY* in loss-of-function *mexZ* mutants bypasses the lengthy activation process of the resistance mechanism and allows a higher fraction of cells to survive rapid shifts in drug concentration. We propose a novel "Response Dynamics" AST assay, which quantifies the recovery of microbial populations following drug exposures and is complementary to MIC.

Results

Single-cell microfluidics shows heterogeneous response to aminoglycosides

To follow physiological changes in a population of single cells in real time as they respond to a step increase in drug concentrations, we developed a microfluidic device that combines mother-machine single-cell trapping with fast media switching[2,33] (**Fig. 1B**). A population of individual "mother cells" are each trapped at the closed end of short narrow chambers connected on their open side to a larger feeding channel where fresh M63 media is flowed. As the cells grow and divide, daughter cells are pushed into the feeding channel and are flushed away, keeping the mother cell in place through many generations. A system of valved inputs allows rapid switching between media with and without drug. We have also engineered mutations to adapt *P. aeruginosa* lab strain PA14 to microfluidic studies, as well as a reporter system to measure the expression of resistance genes (Methods). To measure expression of the *mexXY* operon during responses to aminoglycosides, we have designed a promoter fusion placing a gene coding for mCherry under the regulation of the *mexXY* promoter, as well as fast folding GFP expressed from a constitutive P_{rpoD} promoter, in the same pMQ95 vector[34]. The mCherry fluorescence signal is normalized by the GFP signal, which serves as a control and allows filtering of global effects on transcription. We have transformed this plasmid into a PA14 lab strain, together with motility Δ*flgK*/Δ*pilA* deletions needed to keep the bacteria in the chambers (referred here as WT).

Following an abrupt and sustained exposure to 1000 μg/ml spectinomycin, which is close to the IC_{50} concentration where population-level growth is reduced to half, we observed wide ranges of growth rates and MexXY expression among single cells. While all cells experienced an initial decrease in growth rate, after a few hours many cells started to

recover growth. Some of these growing cells sustained growth and resumed regular cell division, while others lingered in a state of slow growth and irregular division for the duration of the experiment. To compare these subpopulations, we categorized cell fates based on the number of doublings after drug exposure as Recovered (>3), Moribund (1 or 2), or Arrested (0) (**Fig 1C-E**, **S1**). We next asked whether these different cell fates were dictated by the expression of MexXY at the onset of the drug. We followed the fluorescent reporters for MexXY in individual cells during the dynamical response and separated the cells according to their fate. While all cells showed some degree of MexXY upregulation during the response, recovered cells expressed MexXY the fastest, while moribund and arrested cells showed a slower response (**Fig. 1FG**). Recovered cells reached and sustained ~4-fold higher levels of MexXY expression, significantly above moribund or arrested cells (**Fig S1D**). In general, expression of MexXY preceded growth recovery, suggesting that induction of MexXY is indeed necessary for cell survival[26].

To understand whether early expression of resistance can predict recovery, we used an information gain approach to calculate the prediction power of gene expression or growth in the outcome of individual cells (Methods)[2]. Recovery can be reasonably predicted from MexXY expression levels about four hours into the response, when recovered cells start to resume growth (**Fig. 1H**). However, recovery could not be predicted from initial levels of MexXY expression at the time of drug exposure. Therefore, small subpopulations can survive aggressive drug treatments even in homogeneous environments with no detectable pre-existing variations in growth or expression of resistance, and cell fate is determined only after drug exposure. Interestingly, cell growth itself is a better predictor of recovery, predicting cell fates still during the slow growth period following drug exposure. Therefore, cells that retain slightly higher levels of metabolic activity are poised to induce expression of MexXY and recover growth. Next, we investigated the role of MexZ regulation in single cell survival and the emergence of heterogeneity during the drug response.

Loss of MexZ repression increases cell survival upon drug exposure

The effects of *mexZ* mutations on the fitness of *P. aeruginosa* during antibiotic treatments is not clear, as such mutations do not increase resistance by traditional measures[32]. Although a deletion of the gene coding for repressor MexZ has been reported to increase basal levels of MexXY expression in comparison to the wild type, fully induced MexXY levels in the presence of the drug are still similar between the two strains[29]. Since differences in fitness are unlikely to arise during steady-state growth under the drug[30,31], when resistance is fully induced, we investigate the hypothesis that the continuous expression of *mexXY* in loss-of-function *mexZ* mutants bypasses the lengthy activation process of the resistance mechanism and allows a higher fraction of cells to survive rapid shifts in drug concentration. For this, we engineered a Δ*mexZ* strain with a clean deletion of MexZ derived from the same WT strain used in the microfluidic experiment above, as well as a

Δ*mexY* strain with a deletion of efflux pump MexY as a negative control. We then repeated the microfluidic experiment with the Δ*mexZ* and Δ*mexY* mutant strains.

In contrast to the heterogenous response observed in the wild-type strain, the Δ*mexZ* mutant maintained growth upon drug exposure, with all cells surviving (**Fig 2A-C**). Unlike WT cells, which experienced a decrease in growth following exposure prior to induction of MexXY, all Δ*mexZ* cells quickly equilibrated to a slightly lower steady-state growth rate in the presence of the drug. Meanwhile, unsurprisingly, all Δ*mexY* mutant cells quickly stopped growing following exposure, with none recovered. Thus, cell growth recovery depends on MexXY expression and *mexZ* deletions indeed increase single-cell survival to drug exposures. Overall, phenotypic heterogeneity following drug exposure was exclusive to WT cells. While the Δ*mexZ* mutant equilibrated to a growing phenotype and the Δ*mexY* mutant equilibrated to an arrested phenotype, the fate of WT cells spanned the space between these two phenotypes. Therefore, the emergence of heterogeneity depends on MexZ regulation of drug resistance and results from the noisy induction of resistance genes.

Next, we compared the expression of MexXY between WT and Δ*mexZ* mutants (**Fig 2DE**). Δ*mexZ* mutants started with basal levels of MexXY ~2-fold higher than the WT in the absence of drug. After drug exposure, the slight decrease of growth rate in Δ*mexZ* cells corresponded to a slight increase of MexXY levels. Surprisingly, MexXY levels in Δ*mexZ* cells remained significantly below that reached by recovered WT cells (**Fig S1E**). While Δ*mexZ* cells expressed sufficient levels of MexXY prior to the exposure and remained in a similar growth state in the presence of the drug, WT cells only induced MexXY expression after growth was decreased. In these conditions, MexXY can reach higher levels since it is not substantially diluted by cell growth[35]. This result is consistent with other studies where slow growth resulted in higher expression of resistance genes[36,37]. Taken together, these results suggest that sudden drug exposures take a significant toll on WT populations, with only a subpopulation of cells managing to induce resistance and recover growth (**Fig S1F**). Therefore, Δ*mexZ* should have a fitness advantage over the WT in variable environments during the time it takes WT populations to recover growth. Next, we test this hypothesis in competition assays.

Loss of *mexZ* function confers temporary advantage following drug exposure

Although Δ*mexZ* mutant cells have a higher survival rate than the WT during an abrupt exposure to spectinomycin, recovered WT cells that successfully induce MexXY can grow just as fast under sustained drug conditions. Following a sudden drug exposure, faster growing recovered cells tend to dominate the WT population over time, bringing the WT population to a similar growth rate to the Δ*mexZ* mutant. Therefore, we predict that *mexZ* mutations bring only a temporary fitness advantage immediately following drug exposures, which should disappear as conditions stabilize. To test this prediction, we conducted competition experiments using a continuous culture device (chemostat), which

allows the propagation of liquid cultures in carefully controlled environments for many generations (**Fig 3A**). We built a device capable of measuring optical density (OD) and fluorescence, which we use to measure the size of the subpopulation of cells corresponding to the Δ*mexZ* strain, which carries an mKO fluorescent marker[38] (Methods). Therefore, our competition assays with mixed cultures of Δ*mexZ* and WT strains can determine the relative abundance of Δ*mexZ* cells in real time. In each experiment, we also verified the abundance of Δ*mexZ* and WT cells by counting CFUs at select time points.

To determine how growing populations respond to sudden exposure to antibiotics, we started by growing WT, Δ*mexZ*, and Δ*mexY* as monocultures and exposed them to a single, sustained step increase in drug concentration (**Fig 3BC**). We ran these experiments at a relatively low dilution rate of 0.6 $hour^{-1}$, which allowed each strain to stabilize at an OD of ~0.4 in the absence of drug. Following an exposure to 1000 μg/ml spectinomycin, both WT and Δ*mexY* were initially quickly diluted from the culture, close to the rate which would be expected if all cells were arrested. However, while Δ*mexY* was subsequently washed out of the culture, the WT started to recover growth after ~5 hours. Meanwhile, the Δ*mexZ* culture did not experience a sharp decrease in OD and slowly adjusted to growth at a slightly lower OD in the presence of the drug. Although we kept our experiment within 24 hours to prevent the emergence of mutants, both WT and Δ*mexZ* were slowly converging to a similar OD towards the end of the experiment. We saw a similar pattern with an exposure to 700 μg/ml spectinomycin, where the WT was initially diluted but recovered after ~5 hours, while Δ*mexZ* did not experience drastic changes in OD. CFU counts largely followed OD measurements, despite slight differences due to inviable cells counting towards OD but not CFU. Overall, these experiments show that *mexZ* mutations shorten the population-level recovery to abrupt drug exposures.

Next, we competed the Δ*mexZ* mutant with the WT in mixed cultures to determine changes in their relative abundance during drug exposures (**Fig 3DE**). In the absence of drug, both strains were stable at ~50% abundance, indicating that *mexZ* mutations do not bring significant fitness costs under our experimental conditions. After exposures to 700 and 1000 μg/ml spectinomycin, the relative abundance of Δ*mexZ* mutants in the population grew to ~80% over 5 to 10 hours, but then stabilized at these values. These relative abundances were also confirmed by CFU counts. Therefore, *mexZ* mutations indeed provide a temporary fitness advantage in direct competition with the WT. These results suggest that such regulatory mutations are expected to rise in *P. aeruginosa* populations frequently subjected to antibiotic treatments. Next, we developed a simple liquid-culture assay to quantify the fitness advantage provided by fast recovery to drug exposures.

"Response Dynamics" assay to measure population recovery to drug exposures

Since *mexZ* mutations do not provide a clear fitness advantage during steady-state growth in the presence of the antibiotic, the advantage such mutations provide during sudden drug exposures is not captured by traditional measures of resistance obtained by

growing microbial cultures under steady drug conditions. Therefore, we developed a "Response Dynamics" assay to profile antibiotic resistance in a dynamic context. In this assay, growing liquid cultures are suddenly exposed to a sharp increase in drug concentration, which allows us to quantify population-level recovery (**Fig 4A**). The arrest of a large fraction of a growing bacterial culture following a drug exposure is manifested as a pause (or decrease) in population-level growth, during the time it takes for the subpopulation of recovered cells to grow past the background of arrested cells. This pause in growth accounts for the contributions of both cell death and slow growth to the delay in population recovery. In our assay, we expose an array of mid-log phase bacterial cultures to shifts in drug concentrations picked from a gradient, and measure both the duration of the pause in growth following exposure and the growth rate after population growth is resumed. We extract from this assay two complementary measures of resistance: 1) *Dynamical Resistance*, which is the drug concentration that introduces a delay in population-level recovery from drug exposure equivalent to the pre-drug doubling time, and 2) *Steady-State Resistance*, which is the drug concentration that halves the growth rate of the recovered population (similar to the IC_{50} concentration, which correlates with MIC). Our assay captures the dynamical aspect of antibiotic responses, which is critical for resistance and is not measured by MIC assays.

To verify that our Response Dynamics assay can capture the fitness advantage of *mexZ* mutations, we performed the assay in the WT, Δ*mexZ*, and Δ*mexY* strains. Following exposures to high drug concentrations close to the MIC, we observed long delays in growth recovery for WT cultures, while Δ*mexZ* cultures kept growing without interruptions and Δ*mexY* cultures failed to recover growth (**Fig 4B**). However, the steady-state growth rate following recovery was still similar between WT and Δ*mexZ*. Therefore, the heterogeneous behavior of WT cells following drug exposures translates into reliable population-level behaviors that can be quantified.

Next, we calculated steady-state and dynamical resistances. For all strains, both the speed of recovery from drug exposures (**Fig 4C**) and the steady-state growth rate (**Fig 4D**) decline as a function of the spectinomycin dose. While steady-state growth declines rapidly with drug dose for the Δ*mexY* strain, WT and Δ*mexZ* can sustain growth under much higher doses, with the growth rate declining in a very similar manner for both strains. Therefore, the presence of a functional MexXY affords resistance regardless of regulation, giving WT and Δ*mexZ* the same steady-state resistance, which is consistent with the similar MICs reported in the literature[32]. On the other hand, while the Δ*mexZ* strain only showed delays in recovery at high drug doses, the WT showed significant delays at much lower drug doses, only slightly higher than the Δ*mexY* strain. Therefore, the resulting lower dynamical resistance of the WT in comparison to Δ*mexZ* captures its faltering population growth caused by its heterogeneous drug response.

Although steady-state and dynamical resistances measure different properties relating to antibiotic resistance, they are not completely independent, as they depend on the action of the same resistance mechanism. Steady-state resistance relates to the efficiency of resistance mechanisms, measuring their ability to support growth at higher drug concentrations. On the other hand, dynamical resistance relates to the regulation of resistance mechanisms, and measures the ability of cells to quickly activate the appropriate responses upon sudden drug exposures. Therefore, a more efficient resistance mechanism, capable of clearing drug at a higher rate, will increase both measures of resistance. However, slower responses will result in lower dynamical resistance, without necessarily changing steady-state resistance. This is evident by the decrease in dynamical resistance caused by the presence of MexZ regulation, which does not change steady-state resistance (**Fig 4E**). Meanwhile, steady-state and dynamical resistances are similar for Δ*mexZ,* where resistance is constitutively expressed, since growth and speed of recovery start decreasing at similar drug doses. Steady-state and dynamical resistances are also similar for Δ*mexY,* where resistance is absent, as its survival to drug exposures does not depend on the induction of the MexXY response.

Discussion

We have shown that the most common mutation found in clinical *P. aeruginosa* samples, a loss of function of repressor MexZ[27,28], improves antibiotic resistance by increasing single-cell survival and shortening population recovery from abrupt exposures to the drug. This fitness advantage of *mexZ* mutations relates to the dynamics and heterogeneity of drug responses, which are frequently overlooked and are not captured by most standard methods of antibiotic susceptibility testing (AST). This concept does not fall neatly into the currently used terminology describing the many ways microbes can evade antibiotic treatments. The coexistence of growing and arrested bacterial cells in the presence of antibiotics is usually attributed to heteroresistance – as opposed to persistence, where subpopulations survive under the antibiotic without growing[39]. The underlying mechanisms of heteroresistance are generally attributed to some pre-existing heterogeneity of resistance phenotypes in the population (e.g., stochastic genetic switches), which is then selected upon by the drug[40,41]. Here, we report initially homogeneous microbial populations that develop phenotypic diversity only after antibiotic exposures, because recovery depends on the expression of inducible mechanisms. This heterogeneity results from induction of resistance being hindered by the effects of the drug itself, which leads to either cell survival or death/arrest, depending on whether sufficient expression of resistance genes is quickly achieved.

The emergence of heterogeneity during the induction of antibiotic responses is a general phenomenon and has been observed for different drug classes and model systems (**Fig S7**). However, single-cell and population-level behaviors can differ according to the

specificities of each mechanism of drug action and antibiotic resistance[42]. At the population level, decreases in OD are frequently observed when the antibiotic causes cell lysis. At the single cell level, heterogeneity can present as either well-defined cell fates or a more continuous distribution of phenotypes. Here, the *P. aeruginosa* aminoglycoside response resulted in a wide distribution of growth rates and MexXY expression levels in WT cells, spanning the space between the uniform responses in the Δ*mexY* strain, where there is no resistance, and the Δ*mexZ* strain, where resistance is constitutively expressed. Contrastingly, the heterogeneity in the *E. coli* tetracycline response has been reported to quickly resolve into either cell arrest or full growth recovery[2]. Unlike the MexXY resistance mechanism, which has low drug specificity[20] and is slowly induced[26] within a low dynamic range[24,43], the *tet* resistance mechanism is quickly induced to high levels upon drug exposure and provides resistance to drug concentrations ~100-fold higher in comparison to sensitive cells[2]. Therefore, it is likely that fluctuations in *tet* expression have a more dramatic effect on the survival of *E. coli* cells exposed to tetracycline. Nevertheless, regardless of such differences, heterogeneity and the resulting population effects are likely to be general to any scenario where cells need to quickly transition to an alternative phenotype to sustain growth in the presence of a stressor.

To assess the resistance profile of bacterial samples, resistance is typically defined by estimating the minimum inhibitory concentration (MIC) required to inhibit the growth of bulk populations in the presence of antibiotics. However, in recent years, it has become clear that populations that are classified as susceptible by their MIC value may still harbor subpopulations that survive antibiotic treatment[40,44], resulting in discrepancies between resistance profiling in the lab and the outcomes of clinical treatments. While clinical antibiotic treatments are generally well designed to completely clear most infections, short courses of antibiotics such as intravenous or inhalation can be delivered within minutes and result in sharp increases of drug bioavailability at the site of infections[13,45]. Therefore, our Response Dynamics AST assay will be relevant in detecting strains with improved recovery to drug exposures in situations where drug delivery happens at shorter timescales than the induction of antibiotic responses. We note that we use the strain's growth rate in the absence of drug to define both the threshold in steady-state growth used to calculate steady-state resistance (half of the pre-drug growth rate) and the threshold in delay of population recovery used to calculate dynamical resistance (pre-drug doubling time). Therefore, our assay can be used to analyze strains with different growth rates and can be carried in different media conditions. This assay has the potential to identify a new class of regulatory mutations that are common in clinical settings and frequently overlooked by traditional AST methods.

These results help explain how regulatory mutations play a critical role in the evolution of microbes in rapidly changing environments, conferring evolvability to cell responses and allowing quick adaptation across different ecological niches. Regulatory mutations, particularly disruptions of transcriptional repression, are much more easily achieved by

evolution than the specific point mutations necessary to refine resistance proteins[46,47]. Therefore, we expect that regulatory mutations increasing microbial survival to drug exposures are widespread in clinical settings. By maintaining population size and growth during antibiotic treatments, microbes can better evade clearance by the immune system[48], increase tissue invasiveness[49], and are more likely to acquire further mutations increasing resistance[50].

Methods

Media, drugs, and strains. All experiments were conducted in a modified M63 minimal medium (2 g/L $(NH_4)_2SO_4$, 13.6 g/L KH_2PO_4, 0.5 mg/L $FeSO_4 \cdot 7H_2O$) supplemented with 2 g/L glucose, 1 g/L casamino acids, 0.12 mg/L MgSO4, and 0.5 mg/L thiamine. Spectinomycin solutions were freshly made from powder stocks (Gold Bio). Spectinomycin was chosen for these experiments because it is reported to cause high induction of MexXY[51]. All strains used in this study were derived from *P. aeruginosa* PA14. The PA14 Δ*flgK*Δ*pilA* strain used in the microfluidic assays was a gift from the O'Toole lab. The deletion of flagellum hook-associated gene *flgK* and type-4 pilus associated gene *pilA* hinders cell motility to keep cells in place within the device. The PA14 strain carrying 2 chromosomal insertions of mKO, used in the continuous culture experiments, was a gift from the Nadell lab. A detailed description of our strains is provided in the Supplemental Information.

Microfluidic experiments. *P. aeruginosa* cultures were grown overnight in LB, then inoculated into the device and forced into the cell channels by centrifugation. Immediately after inoculation, the microfluidic device was mounted on a Nikon TE2000-E microscope with Perfect Focus, a full incubation chamber, and a CoolSnapHQ Monochrome camera. Cells were allowed to equilibrate in the device for 12 hours before imaging. Image acquisition was performed at 37°C using Nikon NIS-Elements software. Exposures were done at very low illumination intensities to avoid light toxicity, with 2×2 binning for mCherry fluorescence but no binning for GFP fluorescence.

For each *P. aeruginosa* strain, we followed ~40 cells in the microfluidic device, recording cell sizes and fluorescence intensities every 5 min, over 20 hours. Cells were grown in M63 medium until growth was stabilized, then exposed to 1000 μg/mL of spectinomycin. We picked a drug concentration which impairs growth, close to the IC_{50} concentration where population-level growth is reduced to half. Gene expression was measured using a reporter plasmid expressing fluorescent reporters sfGFP (5.6 min maturation time) and mCherry (15 min maturation time) from the native promoters of RpoD and MexY, respectively. All data analysis was based on a custom Matlab image-processing pipeline. For each image, the top cell in each channel was identified and their length and mean fluorescence intensity was calculated. Cell division events were identified by looking for

instances where a cell's length dropped to less than 70% of its previous value (**Fig S1B**). Growth rate was measured in doublings/hour by taking the derivative of $\log_2$(cell length).

Predictive power of an attribute. At the end of an experiment with N cells, the outcomes are divided into N_1 recovered cells and N_2 non-recovered cells ($N_1 + N_2 = N$), and the total information entropy of this system is

$$S_T = s\left(\frac{N_1}{N}\right) + s\left(\frac{N_2}{N}\right), \text{ where } s(p) = -p\log_2(p)$$

At time t, for given value x_i of an attribute x of the cell (MexXY expression, for instance), we divide the population into two subpopulations: N_A cells where $x \leq x_i$, and N_B cells where $x > x_i$. Considering the outcome, the information entropy within each subpopulation at time t is

$$S_A = s\left(\frac{N_{1A}}{N_A}\right) + s\left(\frac{N_{2A}}{N_A}\right) \text{ and } S_B = s\left(\frac{N_{1B}}{B}\right) + s\left(\frac{N_{2B}}{N_B}\right)$$

The information gain of splitting of the original population at x_i is then defined, as

$$G(x_i) = \left[S_T - \left(\frac{N_A}{N}\right)S_A - \left(\frac{N_B}{N}\right)S_B\right]/S_T.$$

If each subpopulation at time t shows roughly the same distribution of outcomes as the final population, then $S_A \approx S_B \approx S_T$ and $G \approx 0$. However, if the population at time t is split along the x_i value that separate between recovered and non-recovered cells, then $S_A \approx S_B \approx 0$ and $G \approx 1$. We define the predictive power of attribute x at time t as the gain obtained from the best split of the population, at the x_i value that maximizes G.

Continuous culture experiments. Experiments were run in a custom-made device, which is further described in the Supplemental Information. Glass vials were coated with Sigmacote (Sigma) to prevent biofilm growth. Vials, vial heads, tubing, and all connections were autoclaved before assembly and after each experiment. Complete sterilization was ensured by running 10% bleach, 70% ethanol, and sterile water consecutively through all tubing and connections prior to each experiment. Experiments were carried out at 37 °C in sterile M63 media. Vials were filled with 15 ml of M63 and used to blank OD measurements. Drug media consisted of M63 media with spectinomycin added to either 700 or 1000 μg/ml, mixed until completely dissolved in solution, and filter sterilized into the container used for the experiment. To achieve an abrupt switch to drug in the chemostat, the cultures were spiked with a drug stock to the desired concentration and the media was immediately swapped from M63 to M63 with spectinomycin. Cultures were constantly diluted at 0.6 hr^{-1} with a media peristaltic pump (Buchler), while the volume in the culture was constantly removed at the same rate with a waste peristaltic pump (Zellweger Analytics). OD and mKO fluorescence readings were taken every 5 min for the duration of the experiment. Samples were taken periodically for CFU counting.

Quantification of relative abundance of strains in continuous cultures. Standard growth curves measuring density (OD, absorbance at 650 nm) and fluorescence for WT and Δ*mexZ*-mKO strains were separately obtained in the continuous culture device without dilution (**Fig S5A**). The plot of mKO fluorescence versus OD shows negligible fluorescence for the WT strain and a linear relationship between fluorescence and OD for the Δ*mexZ*-mKO strain within a window of ODs used in our experiments (**Fig S5B**). The slope of this linear part of the plot was used to determine a conversion factor S between mKO fluorescence and the fraction of OD corresponding to the Δ*mexZ*-mKO strain, which allows us to calculate the relative abundance of Δ*mexZ* during competition with WT. We calculate the relative abundance of Δ*mexZ* in the culture $Z(t) = \frac{S\,F}{O}$, where F is the total fluorescence of the competition culture, S is the conversion factor, and O is the total OD of the competition culture.

Response Dynamics assay. Glycerol stocks were inoculated into LB media and grown overnight, diluted 100-fold in 96-well microtiter plates (Falcon) containing 185 µl of M63 medium per well. To avoid edge effects, the outside perimeter of each plate was not used in analysis. OD (absorbance at 595 nm) was recorded by a plate reader (Synergy Neo-2) every 5 minutes for at least 36 hr. A concentration gradient of spectinomycin was set up over multiple 96-well plates. 15 µl of the spectinomycin gradient was added 30 min after OD was first detected above background. We used custom Matlab scripts to calculate the time required for the culture to double following a drug exposure, as well as the resulting steady-state growth rate of the population after growth was resumed, calculated by linear regression of $\log_2$(OD) during the remaining exponential growth. All relevant data was included in this study and made available online as supplemental data.

Dynamical and Steady-state resistances. From the plate reader experiments, we extract two complementary measures of resistance: 1) *Dynamical Resistance,* which is the drug concentration that introduces a delay of one doubling time in the time to reach one doubling following drug exposure in comparison to the absence of drug, and 2) *Steady-State Resistance*, which is the drug concentration that halves the growth rate of the recovered population (similar to the IC_{50} concentration).

Data Availability

The data that support the findings of this study are openly available. All data and code generated in the study are included in the SI and at our GitHub page: https://github.com/schultz-lab/Response-Dynamics. Further inquiries can be directed to the corresponding authors.

Conflict of Interest

The authors declare that the research was conducted in the absence of any commercial or financial relationships that could be construed as a potential conflict of interest.

Author Contributions

D.S. and D.R. designed the study. D.R. performed the experiments, and D.S. and D.R. analyzed the data. Y.D. created the knockout and reporter plasmids, and D.R. constructed the strains. D.S. and D.R. wrote the manuscript with input from all authors.

Funding

D.S. was supported by grants from NIH/NIGMS P20 GM130454, NSF/PHY 2412766, and an RDP from the CFF (STANTO19R0). D.R. was supported by the Dartmouth PhD Innovation Fellowship program.

Acknowledgements

We thank Chris Geiger and Fabrice Jean-Pierre for important discussions on building our strains and experimental procedures, and Zdenek Svindrych for help with imaging. We also thank Carey Nadell and George O'Toole for gifting us our ancestor strains. Equipment and tools from BioMT were used, which is supported through NIH NIGMS grant P20-GM113132.

References

1. Ramsey, B. W., Dorkin, H. L., Eisenberg, J. D. & al, et. Efficacy of aerosolized tobramycin in patients with cystic fibrosis. *The New England Journal of Medicine* **328**, 1740 (1993).

2. Schultz, D., Palmer, A. C. & Kishony, R. Regulatory Dynamics Determine Cell Fate following Abrupt Antibiotic Exposure. *Cell Systems* **5**, 509-517.e3 (2017).

3. Sánchez-Romero, M. A. & Casadesús, J. Contribution of phenotypic heterogeneity to adaptive antibiotic resistance. *Proceedings of the National Academy of Sciences of the United States of America* **111**, 355–360 (2014).

4. Ehrlich, G. D., Hu, F. Z., Shen, K., Stoodley, P. & Post, J. C. Bacterial plurality as a general mechanism driving persistence in chronic infections. *Clinical Orthopaedics and Related Research* **437**, 20–24 (2005).

5. Dewachter, L., Fauvart, M. & Michiels, J. Bacterial Heterogeneity and Antibiotic Survival: Understanding and Combatting Persistence and Heteroresistance. *Molecular Cell* **76**, 255–267 (2019).

6. Bhagirath, A. Y. *et al.* Cystic fibrosis lung environment and *Pseudomonas aeruginosa* infection. *BMC Pulmonary Medicine* **16**, 1–22 (2016).

7. Nixon, G. M. *et al.* Clinical outcome after early *Pseudomonas aeruginosa* infection in cystic fibrosis. *Journal of Pediatrics* **138**, 699–704 (2001).

8. Pirnay, J.-P. *et al. Pseudomonas aeruginosa* Population Structure Revisited. *PLoS ONE* **4**, e7740 (2009).

9. Cullen, L. *et al.* Phenotypic characterization of an international *Pseudomonas aeruginosa* reference panel: Strains of cystic fibrosis (cf) origin show less in vivo virulence than non-cf strains. *Microbiology* **161**, 1961–1977 (2015).

10. Martínez, J. L. Short-sighted evolution of bacterial opportunistic pathogens with an environmental origin. *Frontiers in Microbiology* **5**, 1–4 (2014).

11. Smith, E. E., Buckley, D. G. & Wu, Z. Genetic adaptation of *Pseudomonas aeruginosa* to the airways of cystic fibrosis patients. *Proc Natl Acad Sci (USA)* **103**, 8487–8492 (2006).

12. Abed, W. H. & Kareem, S. M. Molecular detection of *gyrA* and *mexA* genes in *Pseudomonas aeruginosa*. *Mol Biol Rep* **161**, 7907–7912 (2021).

13. Ratjen, F., Brockhaus, F. & Angyalosi, G. Aminoglycoside therapy against *Pseudomonas aeruginosa* in cystic fibrosis : A review. *Journal of Cystic Fibrosis* **8**, 361–369 (2009).

14. Niels, V., Christian, K. & Niels, H. Prevention of chronic *Pseudomonas aeruginosa* colonisation in cystic fibrosis by early treatment. *The Lancet* **338**, 725–726 (1991).

15. Folkesson, A. *et al.* Adaptation of *Pseudomonas aeruginosa* to the cystic fibrosis airway: An evolutionary perspective. *Nature Reviews Microbiology* **10**, 841–851 (2012).

16. Wong, A., Rodrigue, N. & Kassen, R. Genomics of Adaptation during Experimental Evolution of the Opportunistic Pathogen *Pseudomonas aeruginosa*. *PLoS Genetics* **8**, e1002928 (2012).

17. Krahn, T. *et al.* Determinants of intrinsic aminoglycoside resistance in *Pseudomonas aeruginosa*. *Antimicrobial Agents and Chemotherapy* **56**, 5591–5602 (2012).

18. Sobel, M. L., McKay, G. A. & Poole, K. Contribution of the MexXY multidrug transporter to aminoglycoside resistance in *Pseudomonas aeruginosa* clinical isolates. *Antimicrobial Agents and Chemotherapy* **47**, 3202–3207 (2003).

19. Hocquet, D. *et al.* Relationship between antibiotic use and incidence of MexXY-OprM overproducers among clinical isolates of *Pseudomonas aeruginosa*. *Antimicrobial Agents and Chemotherapy* **52**, 1173–1175 (2008).

20. Morita, Y., Tomida, J. & Kawamura, Y. MexXY multidrug efflux system of *Pseudomonas aeruginosa*. *Frontiers in Microbiology* **3**, 1–13 (2012).

21. Vogne, C., Aires, J. R., Bailly, C., Hocquet, D. & Plésiat, P. Role of the Multidrug Efflux System MexXY in the Emergence of Moderate Resistance to Aminoglycosides among *Pseudomonas aeruginosa* Isolates from Patients with Cystic Fibrosis. *Antimicrobial Agents and Chemotherapy* **48**, 1676–1680 (2004).

22. Morita, Y., Sobel, M. L. & Poole, K. Antibiotic inducibility of the MexXY multidrug efflux system of *Pseudomonas aeruginosa*: Involvement of the antibiotic-inducible PA5471 gene product. *Journal of Bacteriology* **188**, 1847–1855 (2006).

23. Matsuo, Y., Eda, S., Gotoh, N., Yoshihara, E. & Nakae, T. MexZ-mediated regulation of *mexXY* multidrug efflux pump expression in *Pseudomonas aeruginosa* by binding on the *mexZ – mexX* intergenic DNA. *FEMS Microbiol Lett* **238**, 23–28 (2004).

24. Jeannot, K., Sobel, M. L., El Garch, F., Poole, K. & Plésiat, P. Induction of the MexXY efflux pump in *Pseudomonas aeruginosa* is dependent on drug-ribosome interaction. *J Bacteriol* **187**, 5341–5346 (2005).

25. Morita, Y., Gilmour, C., Metcalf, D. & Poole, K. Translational control of the antibiotic inducibility of the PA5471 gene required for *mexXY* multidrug efflux gene expression in *Pseudomonas aeruginosa*. *Journal of Bacteriology* **191**, 4966–4975 (2009).

26. Hocquet, D. *et al.* MexXY-OprM Efflux Pump Is Necessary for Adaptive Resistance of *Pseudomonas aeruginosa* to Aminoglycosides. *Antimicrobial Agents and Chemotherapy* **47**, 1371–1375 (2003).

27. Marvig, R. L., Sommer, L. M., Molin, S. & Johansen, H. K. Convergent evolution and adaptation of *Pseudomonas aeruginosa* within patients with cystic fibrosis. *Nature Genetics* **47**, 57–64 (2015).

28. Guénard, S. *et al.* Multiple mutations lead to MexXY-OprM-dependent aminoglycoside resistance in clinical strains of *Pseudomonas aeruginosa*. *Antimicrobial Agents and Chemotherapy* **58**, 221–228 (2014).

29. Hay, T., Fraud, S., Lau, C. H., Gilmour, C. & Poole, K. Antibiotic Inducibility of the mexXY Multidrug Efflux Operon of *Pseudomonas aeruginosa*: Involvement of the MexZ Anti-Repressor ArmZ. *PLoS ONE* **8**, 20–23 (2013).

30. López-Causapé, C., Rubio, R., Cabot, G. & Oliver, A. Evolution of the *Pseudomonas aeruginosa* Aminoglycoside Mutational Resistome *In Vitro* and in the Cystic Fibrosis Setting. *Antimicrob Agents Chemother* **62**, e02583-17 (2018).

31. Sanz-García, F., Hernando-Amado, S. & Martínez, J. L. Mutational evolution of *Pseudomonas aeruginosa* resistance to ribosome-targeting antibiotics. *Frontiers in Genetics* **9**, 1–13 (2018).

32. Frimodt-Møller, J. *et al.* Mutations causing low level antibiotic resistance ensure bacterial survival in antibiotic-treated hosts. *Scientific Reports* **8**, 1–13 (2018).

33. Wang, P. *et al.* Robust Growth of *Escherichia coli*. *Current Biology* **20**, 1099–1103 (2010).

34. Shanks, R. M. Q., Caiazza, N. C., Hinsa, S. M., Toutain, C. M. & O'Toole, G. A. *Saccharomyces cerevisiae*-based molecular tool kit for manipulation of genes from gram-negative bacteria. *Applied and Environmental Microbiology* **72**, 5027–5036 (2006).

35. Klumpp, S., Zhang, Z. & Hwa, T. Theory Growth Rate-Dependent Global Effects on Gene Expression in Bacteria. *Cell* **139**, 1366–1375 (2009).

36. Stevanovic, M., Carvalho, J. P. T., Bittihn, P. & Schultz, D. Dynamical model of antibiotic responses linking expression of resistance genes to metabolism explains emergence of heterogeneity during drug exposures. *Physical Biology* **21**, 036002 (2024).

37. Møller, T. S. B. *et al.* Relation between *tetR* and *tetA* expression in tetracycline resistant *Escherichia coli*. *BMC Microbiol* **16**, 39–46 (2016).

38. Toprak, E. *et al.* Building a morbidostat: an automated continuous-culture device for studying bacterial drug resistance under dynamically sustained drug inhibition. *Nature Protocols* **8**, 555–567 (2013).

39. Balaban, N. Q., Merrin, J., Chait, R., Kowalik, L. & Leibler, S. Bacterial Persistence as a Phenotypic Switch. *Science* **305**, 1622–1625 (2004).

40. Band, V. I. & Weiss, D. S. Heteroresistance: A cause of unexplained antibiotic treatment failure? *PLoS Pathogens* **15**, 1–7 (2019).

41. Andersson, D. I., Nicoloff, H. & Hjort, K. Mechanisms and clinical relevance of bacterial heteroresistance. *Nature Reviews Microbiology* **17**, 479–496 (2019).

42. Pang, Z., Raudonis, R., Glick, B. R., Lin, T. J. & Cheng, Z. Antibiotic resistance in *Pseudomonas aeruginosa*: mechanisms and alternative therapeutic strategies. *Biotechnology Advances* **37**, 177–192 (2019).

43. Lau, C. H. F., Krahn, T., Gilmour, C., Mullen, E. & Poole, K. AmgRS-mediated envelope stress-inducible expression of the *mexXY* multidrug efflux operon of *Pseudomonas aeruginosa*. *Microbiology Open* **4**, 121–135 (2015).

44. Sánchez-Romero, M. A. & Casadesús, J. Contribution of phenotypic heterogeneity to adaptive antibiotic resistance. *Proceedings of the National Academy of Sciences of the United States of America* **111**, 355–360 (2014).

45. Geller, D. E., Pitlick, W. H., Nardella, P. A., Tracewell, W. G. & Ramsey, B. W. Pharmacokinetics and Bioavailability of Aerosolized Tobramycin in Cystic Fibrosis. *Chest* **122**, 219–226 (2002).

46. Shou, C. *et al.* Measuring the Evolutionary Rewiring of Biological Networks. *PLoS Comput Biol* **7**, e1001050 (2011).

47. Ali, F. & Seshasayee, A. S. N. Dynamics of genetic variation in transcription factors and its implications for the evolution of regulatory networks in Bacteria. *Nucleic Acids Res* **48**, 4100–4114 (2020).

48. Fraud, S. & Poole, K. Oxidative Stress Induction of the MexXY Multidrug Efflux Genes and Promotion of Aminoglycoside Resistance Development in *Pseudomonas aeruginosa*. *Antimicrobial Agents and Chemotherapy* **55**, 1068–1074 (2011).

49. Laborda, P. *et al.* Mutations in the efflux pump regulator MexZ shift tissue colonization by *Pseudomonas aeruginosa* to a state of antibiotic tolerance. *Nat Commun* **15**, 2584 (2024).

50. Seupt, A., Schniederjans, M., Tomasch, J. & Häussler, S. Expression of the MexXY Aminoglycoside Efflux Pump and Presence of an Aminoglycoside-Modifying Enzyme in Clinical *Pseudomonas aeruginosa* Isolates Are Highly Correlated. *Antimicrobial Agents and Chemotherapy* **65**, e01166-20 (2020).

51. Poole, K., Lau, C. H.-F., Gilmour, C., Hao, Y. & Lam, J. S. Polymyxin Susceptibility in *Pseudomonas aeruginosa* Linked to the MexXY-OprM Multidrug Efflux System. *Antimicrob Agents Chemother* **59**, 7276–7289 (2015).

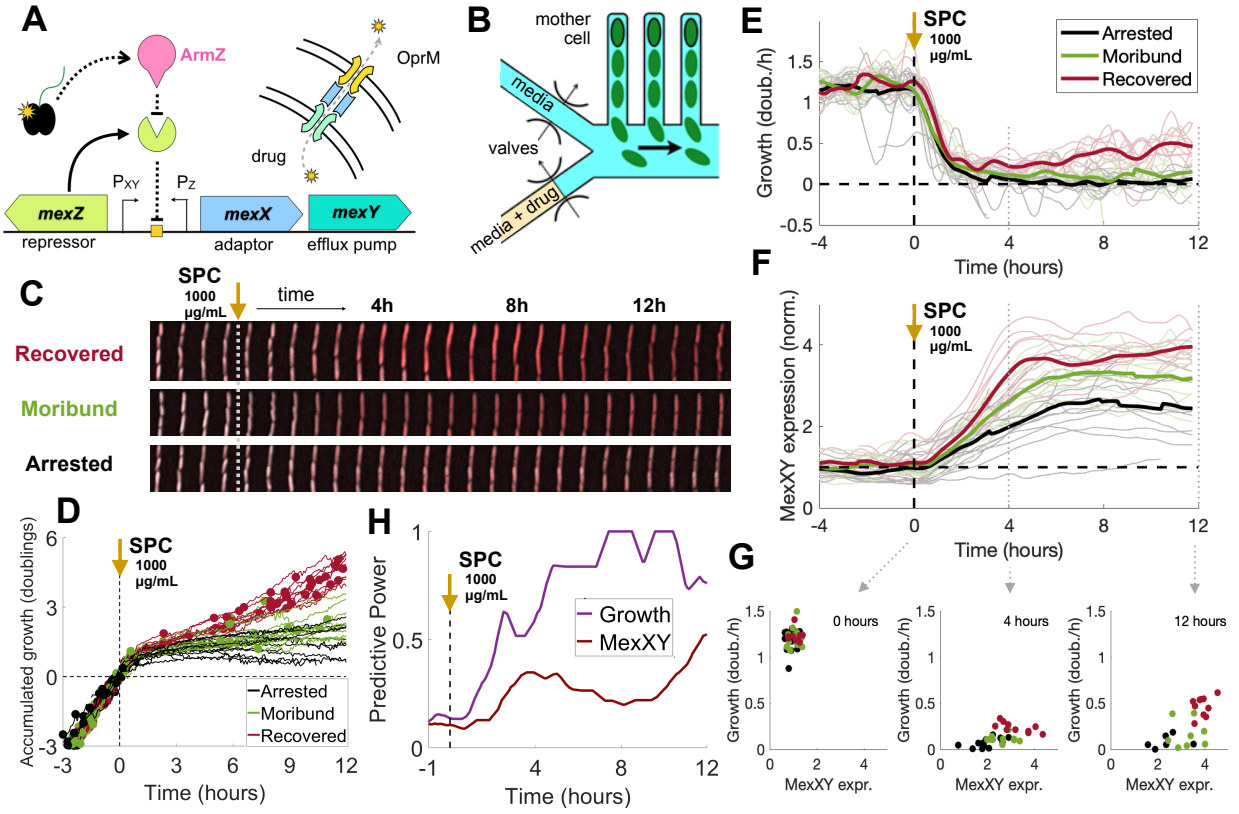

Figure 1 - Abrupt exposure of single WT cells to spectinomycin shows heterogeneous response. (A) *mexXYZ* resistance mechanism: aminoglycoside spectinomycin (SPC), a translation inhibitor, diffuses across the cell membrane and binds ribosome. A decrease in translation efficiency induces expression of anti-repressor ArmZ, which binds repressor MexZ and releases expression of adaptor protein MexX and efflux pump MexY. The multidrug efflux system composed of MexX, MexY, and outer membrane protein OprM exports spectinomycin out of the cell. **(B)** Design of the microfluidic device, which places single cells in fixed locations as they go through division cycles. Valves allow on-chip rapid switching of media. WT cells carrying the native resistance mechanism with fluorescent reporters were exposed to a step increase of 1000 µg/mL SPC. **(C)** Time courses of individual cells representing the three different cell fates observed: recovered, moribund, and arrested. These cell fates are based on number of division events after drug exposure: recovered cells show 3 or more divisions, moribund cells show 1 or 2 divisions, and arrested show no divisions. **(D)** Accumulated growth in cell length for all cells observed, colored by cell fate and with division events indicated by dots. **(E)** Growth rate in each cell, with cell fate indicated by color. The thick line represents the average growth of cells with similar fate. **(F)** Expression of MexXY in each cell, with cell fate indicated by color. The thick line represents the average expression of cells with similar fate. **(G)** MexXY levels and growth rate at three time points following exposure to spectinomycin, showing the distinct expression pattern of each cell fate. **(H)** Predictive power of cell growth and expression of MexY in determining recovery during early response. Cell growth predicts recovery within the first two hours following exposure, before predictions from MexY. Pre-exposure growth and MexY levels are not predictive of recovery.

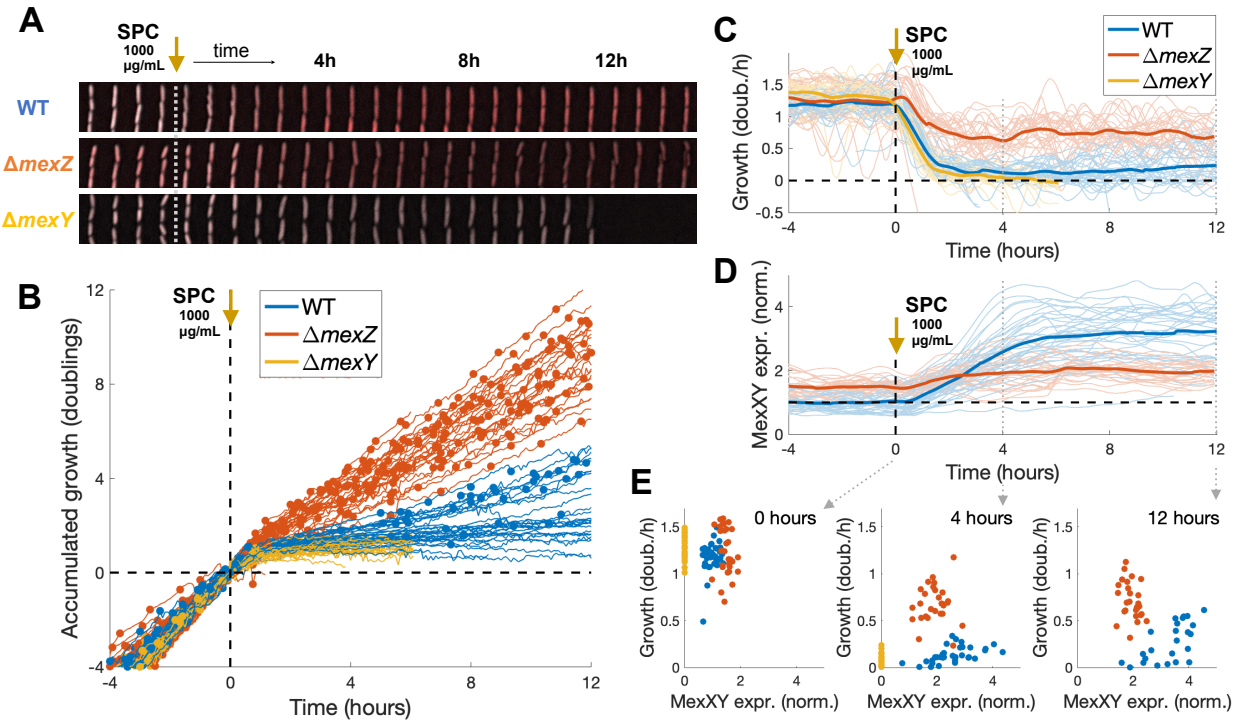

Figure 2 - *mexZ* deletion increases single-cell survival to spectinomycin exposures. **(A)** Time courses of individual WT PA14, Δ*mexZ*, and Δ*mexY* cells following an exposure to 1000 µg/mL spectinomycin in the microfluidic device. **(B)** Accumulated growth in cell length for WT, Δ*mexZ*, and Δ*mexY* cells, colored by genotype, with division events indicated by dots. **(C)** Growth rate in each cell, with genotype indicated by color. The thick line represents the average growth of cells within each genotype. **(D)** Expression of MexXY in each cell, with genotype indicated by color. The thick line represents the average expression of cells within each genotype. **(E)** MexXY levels and growth rate at three time points following exposure to spectinomycin, showing the distinct expression pattern of each genotype.

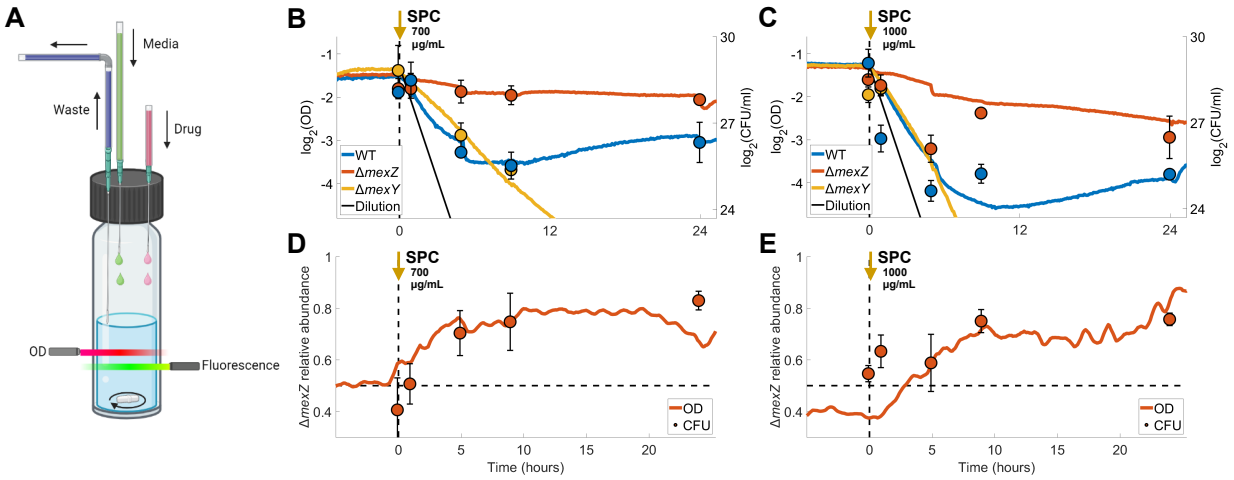

Figure 3 - *mexZ* mutants have a temporary fitness advantage over the WT following drug exposure. (A) Continuous culture system (chemostat) dilutes culture with fresh media at a fixed rate, while keeping the culture at the same volume by removing spent media. OD and fluorescence are measured every 5 minutes. After growth is stabilized in fresh M63 medium, drug is quickly added to the culture to the desired concentration, and medium is switched to M63 with drug for the duration of the experiment. **(B-C)** Monocultures of Δ*mexZ*, Δ*mexY*, and WT exposed to **(B)** 700 and **(C)** 1000 µg/mL spectinomycin. Lines represent OD measurements in the chemostat. Dots represent the CFU counts of 3 plate replicates. **(D-E)** Δ*mexZ* and WT competition in mixed culture during **(D)** 700 and **(E)** 1000 µg/mL spectinomycin exposures. Lines represent the relative abundance of Δ*mexZ*, calculated from fluorescence and OD measurements in the chemostat (Methods). Dots represent the relative abundance of Δ*mexZ* in CFU counts of 3 plate replicates.

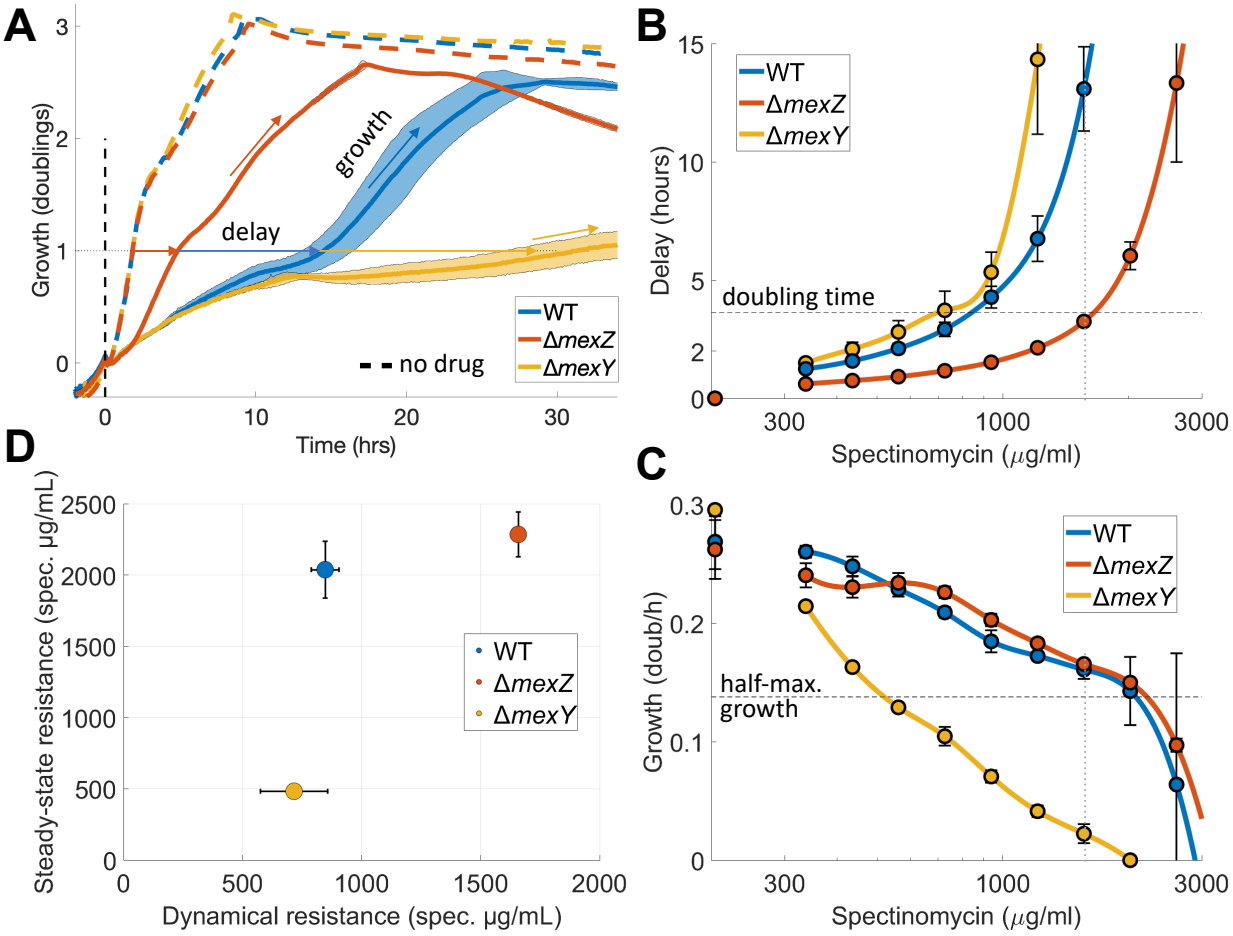

Figure 4 - Steady-state resistance and dynamical resistance describes the antibiotic resistance profile of *Pa*. (A) Growth of WT, Δ*mexZ*, and Δ*mexY* strains upon exposure to a step increase of 1600 μg/mL spectinomycin (at time zero). Horizontal arrows indicate the delay in the time taken to reach one doubling in comparison to growth in the absence of drug. Inclined arrows indicate the steady-state growth reached after population recovery. **(B)** Growth delays of each strain as a function of the spectinomycin dose used in the exposure. The horizontal line indicates the doubling time of these strains during exponential growth in the absence of drug. We calculate *Dynamical Resistance*, which measures the population-level capacity for quick recovery following drug exposure, as the drug concentration that causes an increase equivalent to the doubling time in the time taken to reach one doubling after exposure. The horizontal line shows the drug concentration used in (A). **(C)** Steady-state growth of each strain as a function of the spectinomycin dose used in the exposure. The horizontal line indicates half of the growth rate during exponential growth in the absence of drug. We calculate *Steady-state Resistance*, which measures the capacity for steady-state growth in the presence of drug, as the drug concentration that halves the maximum growth rate reached after exposure. The horizontal line shows the drug concentration used in (A). **(E)** Dynamical and Steady-state resistances for the WT, Δ*mexZ*, and Δ*mexY* strains. *mexZ* deletion increases Dynamical resistance without affecting Steady-state resistance.

Supplemental Information

Common regulatory mutation increases single-cell survival to antibiotic exposures in *Pseudomonas aeruginosa*.

David Ritz[1], Yijie Deng[2], Daniel Schultz[1]
[1] Department of Microbiology & Immunology, Geisel School of Medicine, [2] Thayer School of Engineering – Dartmouth College, Hanover, NH 03755, USA.

Fabrication of the microfluidic device

The device was fabricated by aligning a layer of 25 µm height containing the flow channels and a layer of 1.5 µm height containing the single-cell traps. The master mold was fabricated by ultraviolet photolithography using standard methods. SU-8 (Microchem) photoresist was applied to a silicon wafer by spin coating to appropriate thickness corresponding to the channel height, and patterns were then created by exposing the uncured photoresist to ultraviolet light through custom masks. We used a quartz mask for finer features (Toppan) and a film mask for the flow channels (CAD/Art Services). PDMS monomer (Sylgard 184) with 1:10 curing agent was mixed and poured on top of the wafer mold and air bubbles were removed using a vacuum chamber. After baking at 65°C for 3 hours, the PDMS was peeled off and inlet holes were introduced using a biopsy punch to connect the flow channels to the external tubing. Individual chips were then cut and bonded onto KOH-cleaned 1.5 coverslip slides (VWR) using oxygen plasma treatment, followed by 30 min on an 80°C hotplate and post-baked at 65°C overnight. Media was pumped through the device using a custom-built system that applies air pressure to media containers to induce flow through the device. We used an Arduino to control airflow through solenoid valves, allowing us to switch the pressures applied to containers of media with and without drug. The media inlets both feature high flow resistance channels to prevent backflow and have a short length of contact to prevent mixing (Supplemental Video S1).

Fabrication of the continuous culture device

The main body of the device is a custom-built 3D printed (Stratasys J55) housing, which has a central section to hold a glass vial containing the culture and a 4-pronged magnetic stirbar (IKA Works), as well as slots for LEDs and filter sets to measure two fluorescence channels, a 650 nm laser (Quarton) to measure OD, 3 photodiodes (TT Electronics) to quantify the fluorescence and OD readings, and a 3-D printed base stand underneath the main body, which houses a motor attached to magnetic beads to stir the culture. mKO fluorescence was quantified using a 525-50 nm emission filter (Chroma), a 600-50 nm excitation filter (Chroma), and 530 nm LED light source (LUXEON Star). We performed

the experiments on a PA14 strain that has 2 chromosomal insertions of mKO (Fig. S4D). To amplify the photodiode signals, we used an inverting amplification circuit for OD quantification and an inverting amplification followed by a non-inverting amplification circuit for the fluorescence readings. A Raspberry Pi with a data acquisition board (Pi-Plate) was used to acquire fluorescence and OD measurements and to control the culturing system, using custom-built software.

Construction of plasmids and knockout strains

A *mexXY* reporter plasmid construct (P*mexXY*-YFP-P*rpoD*-CFP) was ordered from Genewiz and used as a base for our reporter system. Our reporter plasmid (DA350) uses a superfolder green fluorescent protein gene (sfGFP)[1], positioned downstream of the P*rpoD* to serve as a reference signal, and a red fluorescent protein gene (mCherry)[2] fused downstream of the *mexXY* promoter to measure its activity. The sfGFP gene was amplified via PCR from plasmid DA313[3] using primers P-GFP-F and P-GFP-R, while the mCherry gene was similarly amplified from plasmid JF72[4] using primers P-RFP-F and P-RFP-R. The backbone fragments were PCR amplified by primers sets P-bk-F1/P-bk-R1, P-bk-F2/P-bk-R2, and P-bk-F3/P-bk-R3, respectively, using P*mexXY*-YFP-P*rpoD*-CFP as template. All PCR fragments were purified and assembled into plasmids using the Gibson assembly method. Following transformation into competent *E. coli* NEB10beta cells (NEB), the resultant transformants were selected for ampicillin resistance by plating onto LB agar plates supplemented with 100 µg/mL of ampicillin. The accuracy of all plasmid sequences was confirmed by Sanger DNA sequencing. This new reporter plasmid offered improved resolution over background fluorescence in *P. aeruginosa*, enabling more accurate measurement of P*mexXY* promoter activity.

The plasmids used to knock out *mexZ* and *mexY* genes from *P. aeruginosa* PA14 strain were constructed using pMQ30 as backbone[5]. The ~1kb upstream and downstream fragments of the target gene were PCR amplified from genomic DNA of PA14 and Gibson assembled into the backbone of pMQ30. Plasmid DA354 was created to knock out *mexZ*. Specifically, two backbone fragments were amplified via PCR from PMQ30 using primer sets Mq-bk-F1/Mq-bk-R1 and Mq-bk-F2/Mq-bk-R2. The upstream and downstream DNA regions of *mexZ* were PCR amplified with primer sets Z-up-F/Z-up-R and Z-dw-F/Z-dw-R, respectively. The four fragments were assembled to make the resultant plasmid DA354. Similarly, plasmid DA355 was constructed by fusing the upstream and downstream DNA regions of *mexY*, together with the same pMQ30 backbone. The upstream and downstream regions of *mexY* were PCR amplified with primer sets Y-up-F/Y-up-R and Y-dw-F/Y-dw-R, respectively. The constructs were then transformed into *E. coli* NEB10beta cells (NEB) and spread onto LB plates with gentamicin (10 µg/mL). Following a 24-hour incubation period at 30°C, resistant colonies were selected and propagated in LB broth supplemented with the same antibiotic at 30°C, facilitating plasmid extraction.

Subsequently, the purified plasmids were verified through Sanger sequencing to ensure accuracy.

The Δ*mexZ* and Δ*mexY* knockout strains were generated through in-frame deletions to avoid any potential downstream polar effects, using the above plasmids DA354 and DA355, respectively. The gene knockout followed a previous published two-step allelic exchange protocol[6]. Briefly, the plasmid was first transformed to *E. coli* S17 strain, after which it was conjugated with *P. aeruginosa* PA14 and selected for gentamicin resistance at 30 μg/mL. The knockout out mutants were then subjected to counter selection using sucrose. The right knockout mutants were confirmed by colony PCR[6].

All plasmids were constructed by Gibson assembly[7] using NEBuilder® HiFi DNA Assembly kit (NEB). PCR reactions were conducted using high-fidelity Q5 DNA polymerase (NEB) and the products were purified prior to Gibson assembly. All PCR primers used in this study are listed in Supplemental Table S1. When necessary, primers were specifically designed to include overlapped regions for the assembly process. The assembled plasmids were transformed into chemically competent *E. coli* NEB10beta cells (NEB) and selected for appropriate antibiotic resistances. Plasmids, PCR products, and DNA fragments from agarose gel were purified with Qiagen miniprep, PCR purification, and Gel extraction kits, respectively.

Supplemental Table 1 - List of PCR primers used in this study.

Primers	Sequences 5'-----3'
P-GFP-F	tttgtaaagtagacctaaggagtaaatatgagcaaaggagaagaacttttcactgg
P-GFP-R	ccgatcaagtcttcgcgatgattattatttgtagagctcatccatgccatgtgt
P-RFP-F	acccccggtgcagaaaataaggaggaaaaaaaaatggtgagcaagggcgaaga
P-RFP-R	gacctgcattacttgtacagctcgtccatgccgc
P-bk-F1	gcggcatggacgagctgtacaagtaatgcaggtcgtctcggatcgagaagg
P-bk-F2	ggtgatgacggtgaaaacctctga
P-bk-F3	gctcatatttactccttaggtctactttacaaaaaataagcagaggattatacctgatg
P-Bk-R1	tcagaggttttcaccgtcatcaccgaaacgc
P-bk-R2	ataataatcatcgcgaagacttgatcggtgccgggat
P-bk-R3	tattttctgcaccgggggtgtccctcgattc
Y-up-F	tcagaccgcttctgcgttctgacccttgaaggcggccctgga
Y-up-R	agcaccggcggcgcgatgtcc
Y-dw-F	acatcgcgccgccggtgctggtaccgctgttcttcctgg
Y-dw-R	tgcgttggccgattcattcaggacggcgaattgctgcgac
Mq-bk-F1	gttccgcgcacatttccccgaaacctctgacacatgcagctcccgg
Mq-bk-F2	ctgaatgaatcggccaacgcacgggaagag
Mq-bk-R	tcagaacgcagaagcggtctgat
Mq-bk-R2	ttcggggaaatgtgcgcggaacc
Z-up-F	gttttatcagaccgcttctgcgttctgagcacgcatggcgatggtg
Z-up-R	aggtagggagaactgcgcaggctgtcgcgggttttctgggattc
Z-dw-F	agcctgcgcagttctccct
Z-dw-R	tcccgtgcgttggccgattcattcaggaacggcgcgtagagctgg

References

1. Pédelacq, J.-D., Cabantous, S., Tran, T., Terwilliger, T. C. & Waldo, G. S. Engineering and characterization of a superfolder green fluorescent protein. *Nat. Biotechnol.* **24**, 79–88 (2006).

2. Shaner, N. C. *et al.* Improved monomeric red, orange and yellow fluorescent proteins derived from *Discosoma* sp. red fluorescent protein. *Nat. Biotechnol.* **22**, 1567–1572 (2004).

3. Deng, Y., Beahm, D. R., Ran, X., Riley, T. G. & Sarpeshkar, R. Rapid modeling of experimental molecular kinetics with simple electronic circuits instead of with complex differential equations. *Front. Bioeng. Biotechnol.* **10**, 1–21 (2022).

4. Zeng, J. *et al.* A Novel Bioelectronic Reporter System in Living Cells Tested with a Synthetic Biological Comparator. *Sci. Rep.* **9**, 7275 (2019).

5. Shanks, R. M. Q., Caiazza, N. C., Hinsa, S. M., Toutain, C. M. & O'Toole, G. A. *Saccharomyces cerevisiae*-based molecular tool kit for manipulation of genes from gram-negative bacteria. *Appl. Environ. Microbiol.* **72**, 5027–5036 (2006).

6. Hmelo, L. R. *et al.* Precision-engineering the *Pseudomonas aeruginosa* genome with two-step allelic exchange. *Nat. Protoc.* **10**, 1820–1841 (2015).

7. Gibson, D. G. *et al.* Enzymatic assembly of DNA molecules up to several hundred kilobases. *Nat. Methods* **6**, 343–5 (2009).

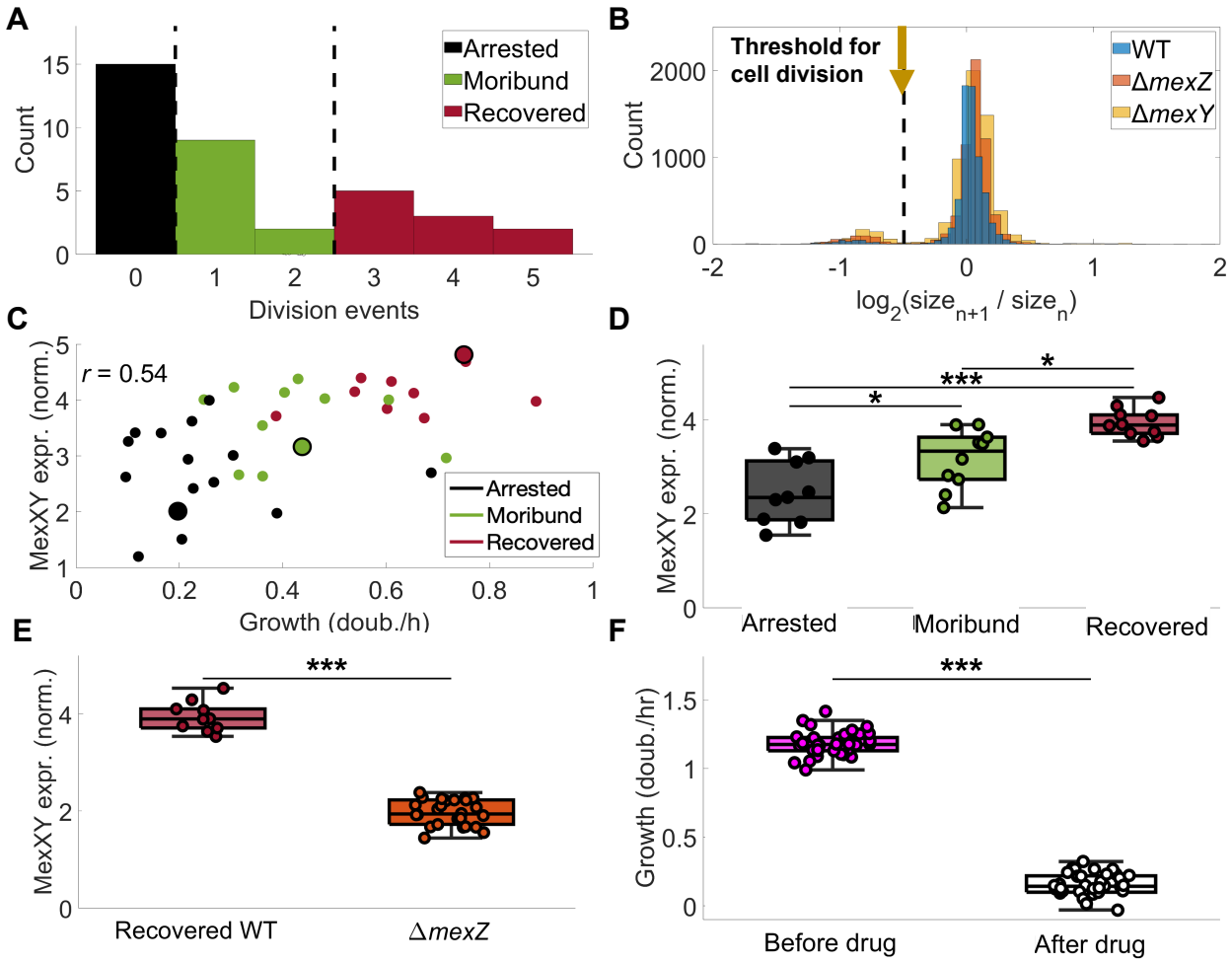

Supplementary Figure 1 - Heterogeneous cell growth and gene expression in the microfluidic experiment. (A) Histogram showing number of division events in each cell following drug exposure in the microfluidic assay. We classify cells into “Recovered” (3 or more division events), “Moribund” (1 or 2 divisions), and “Arrested” (no divisions). **(B)** Histogram of cell sizes relative to their size at the previous time step (5 minutes earlier), throughout the whole experiment for all genotypes in the microfluidic assay. The dotted line depicts the threshold used to identify division events. **(C)** Maximum MexXY expression and final growth rate of all WT cells. The Recovered, Moribund, and Arrested cells depicted in Fig 1C in the main text are denoted by large dots. Pearson’s correlation coefficient shows modest correlation between final levels of MexXY expression and growth rate. **(D)** Comparison of final MexXY expression of Recovered, Moribund, and Arrested WT cells. Normal distribution for each cell fate was determined using a Kolmogorov-Smirnov test with an alpha value of 0.05. ANOVA was performed, and each pairwise comparison was checked for significance. Multiple comparisons were corrected using the Dunn–Šidák correction**. (E)** Comparison of final MexXY expression of Recovered WT cells and Δ*mexZ* cells. **(F)** Comparison of all WT cells’ growth rates before and after drug exposure. For panels E-F, a two-way t-test was performed with an alpha value of 0.05. The asterisks for panels D-F denote *** $p < 0.001$, ** $p < 0.01$, * $p < 0.05$.

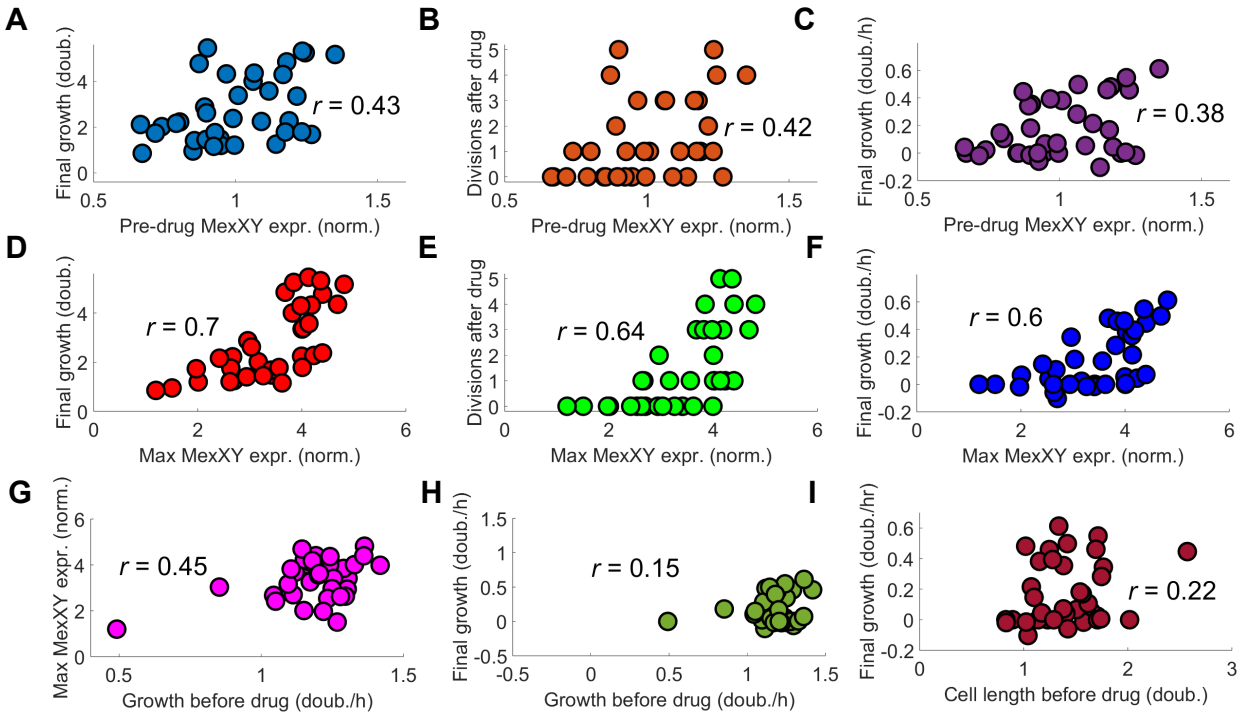

Supplementary Figure 2 - Induction of MexXY expression promotes recovery of cell growth following antibiotic exposure. In WT cells tracked in the microfluidic device, **(A)** accumulated growth, **(B)** division events, and **(C)** final growth rate have a weak positive correlation with MexXY expression at the moment of drug exposure. However, **(D)** accumulated growth, **(E)** division events, and **(F)** final growth rate have a moderate to high positive correlation with the maximum MexXY level reached after drug exposure. **(G)** MexXY expression and **(H)** final growth rate similarly do not correlate with the growth rate at the time of drug exposure. **(I)** The final growth rate also does not correlate with cell length at the moment of drug exposure. Pearson's correlation coefficient is displayed on each graph.

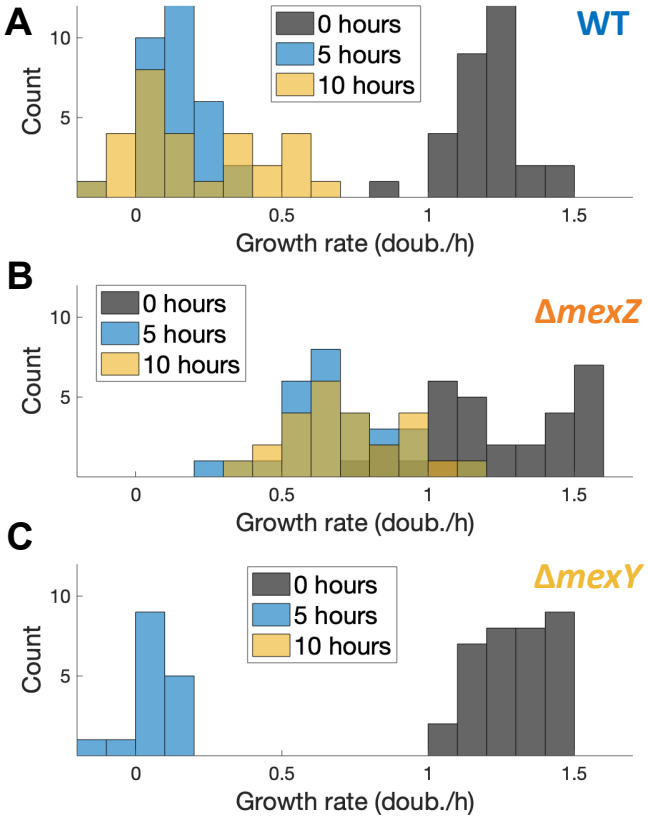

Supplementary Figure 3 - *mexZ* deletion increases survival to an abrupt exposure to spectinomycin. Histogram showing distribution of growth rates for **(A)** WT, **(B)** Δ*mexZ*, and **(C)** Δ*mexY* cells following exposure to 1000 µg/mL spectinomycin in the microfluidic assay. Histograms are shown at the time of exposure (0 hours), as well as 5 and 10 hours afterwards. WT cells display a significant reduction of growth followed by heterogeneous recovery, while Δ*mexZ* cells maintain growth throughout the experiment.

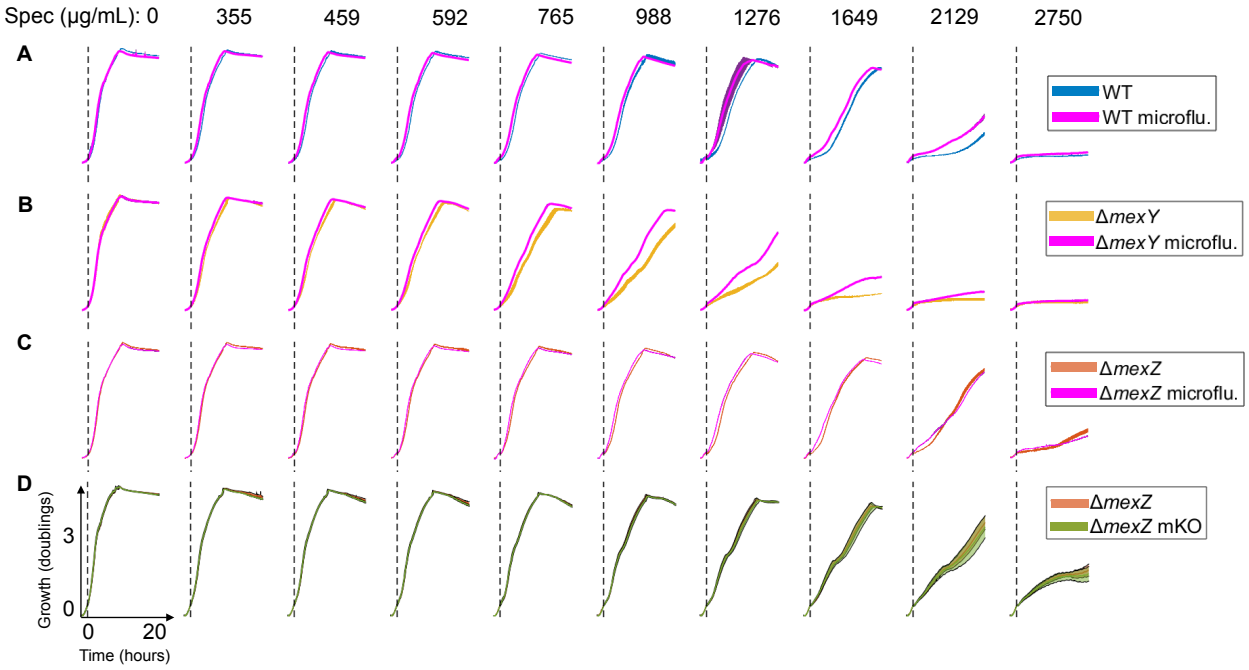

Supplementary Figure 4 - Deletion of motility genes, reporter plasmids, and mKO chromosomal insertions do not affect *P. aeruginosa*'s growth or spectinomycin resistance. Comparison of growth in **(A)** WT, **(B)** Δ*mexY*, and **(C)** Δ*mexZ* strains to their counterparts used in the microfluidic assays, which have a deletion of motility genes and contain a MexXY reporter plasmid. The dotted lines denote abrupt additions of spectinomycin at the doses specified above the panels. We did not detect significant differences in cell growth or resistance. **(D)** Similarly, the Δ*mexZ* strain used in the continuous cultures, which carries 2 chromosomal insertions of mKO, shows similar growth and resistance profile as the Δ*mexZ* strain from which it is derived. The shading around each line graph represents the maximum and minimum of two replicates.

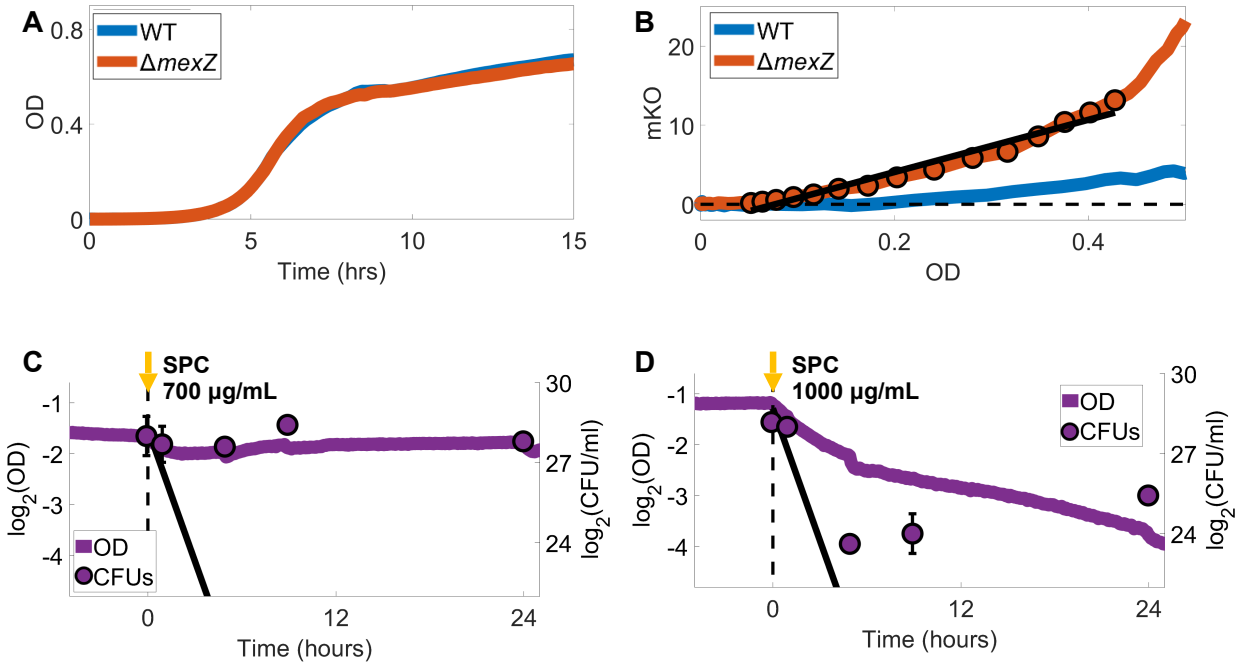

Supplementary Figure 5 - Calibration of the continuous culturing device. (A) Growth of monocultures of a WT strain and a Δ*mexZ* strain with two chromosomal insertions of mKO, in the absence of dilution. **(B)** Fluorescence measured from the Δ*mexZ* strain increases linearly with OD within the range used in our experiments. The slope of the black fitted line overlaid on Δ*mexZ*'s standard curve was used to determine Δ*mexZ*'s relative abundance during competition assays in Fig 3DE in the main text (Methods). Competition cultures were kept at 0.4 OD or below, minimizing the effect of WT auto-fluorescence on readings. **(C-D)** Total OD of the mixed culture during the competition assays between WT and Δ*mexZ* under **(C)** 700 µg/mL and **(D)** 1000 µg/mL spectinomycin, from Fig 3DE in the main text. Dotted line denotes the moment of drug exposure. Black line denotes the limit of dilution in the absence of growth.

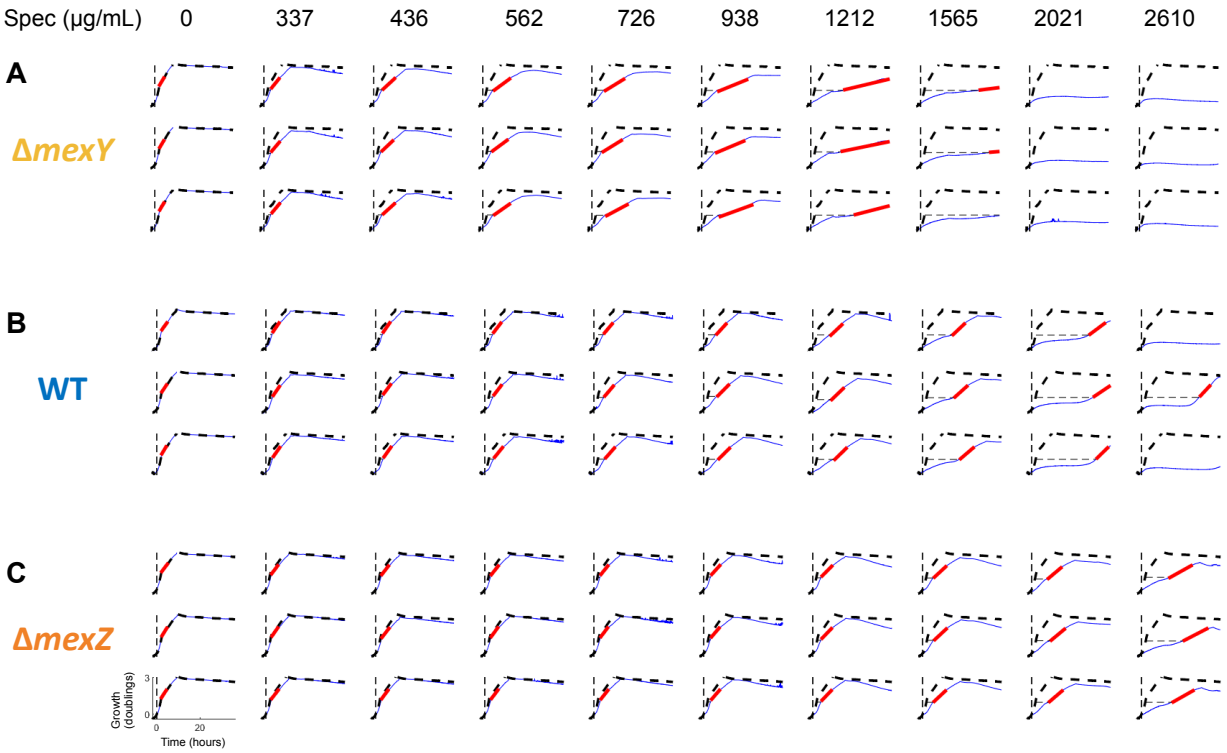

Supplementary Figure 6 - Calculation of Steady-State and Dynamical resistances from cell growth during an abrupt drug exposure. Growth curves of **(A)** Δ*mexY*, **(B)** WT, and **(C)** Δ*mexZ* cells following exposure to spectinomycin concentrations picked from a gradient, performed in three replicates. The red line shows the steady-state growth following population recovery, which was used to calculate Steady-state resistance. The horizontal dotted line shows the delay in growth recovery in comparison to the absence of drug, which was used to calculate Dynamical resistance. The overlaid black dotted line represents growth in the absence of drug, which is the first column of each row. These growth curves were used to calculate delays and steady-state growth in Fig 4B-D in the main text.

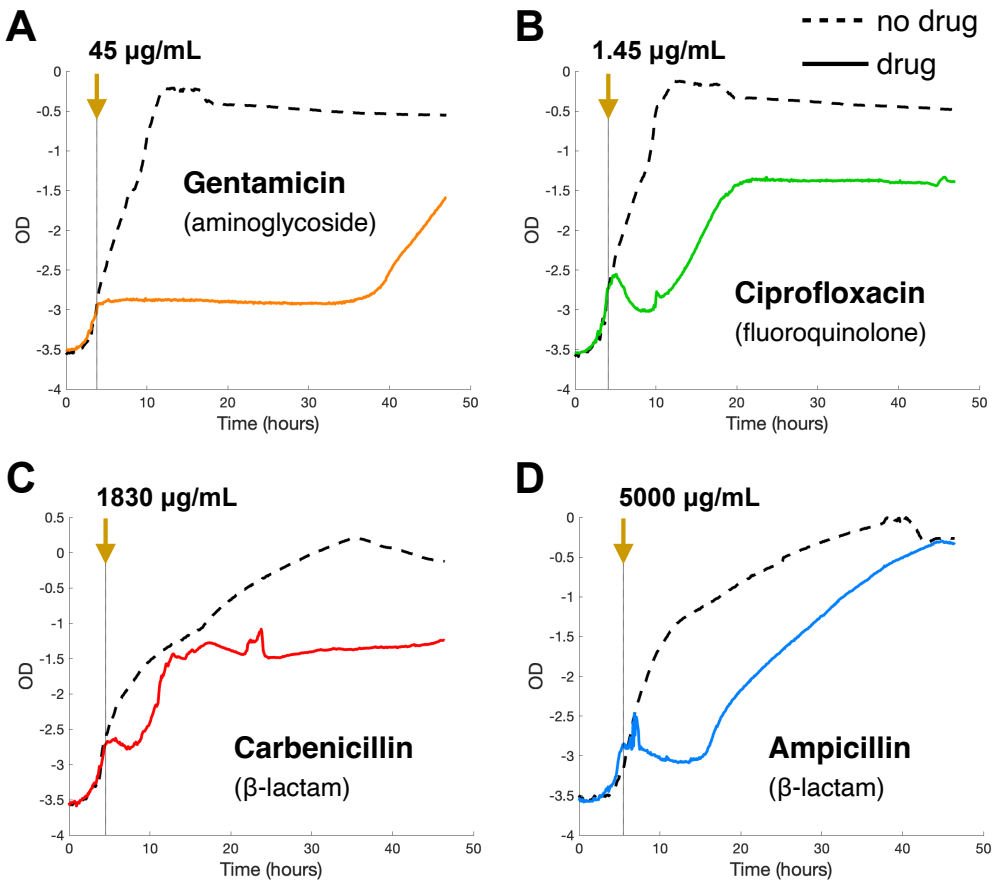

Supplementary Figure 7 – Delay in population-level growth recovery is general across different strains and drug classes. Growth curves of *P. aeruginosa* strain PAO1 following exposures to **(A)** gentamicin (aminoglycoside) and **(B)** ciprofloxacin (fluoroquinolone). Growth curves of *P. aeruginosa* strain PA14 following exposures to **(C)** carbenicillin (β-lactam) and **(D)** ampicillin (β-lactam). The vertical dotted line shows the time of drug exposure. Fluoroquinolones and β-lactams are bactericidal drugs and often result in a reduction of OD following exposure.

Supplementary Video 1- Microfluidic device allows rapid switching between media. In the slowed video, the top media stream is composed of water (no color) and the bottom media stream is composed of water with fluorescein (green color). Both fluid streams are laminar and meet for a short distance, causing minimal mixing. By switching the pressure applied to each media container, we can rapidly select which medium reaches the channel feeding the single-cell traps.

Supplementary Video 2 - Diversity of fates in WT single cells responding to a step increase in spectinomycin concentration. WT cells carrying the native *mexXY* resistance mechanism were exposed to a step increase of 1000 µg/mL spectinomycin at time zero. A fluorescent reporter with a matching promoter was used to measure expression of the efflux pump component MexY (red, mCherry). Imaging was done in a microfluidic device that places single cells in fixed locations as they go through division cycles. Valves allow on-chip rapid switching of media.

Supplementary Video 3 - Δ*mexZ* cells survive a step increase in spectinomycin concentration. Cells carrying a Δ*mexZ* deletion were exposed to a step increase of 1000 µg/mL spectinomycin at time zero. Unlike WT cells, all Δ*mexZ* cells survived the exposure and maintained growth under the drug.

Supplementary Video 4 - Δ*mexY* cells do not survive a step increase in spectinomycin concentration. Cells carrying a Δ*mexY* deletion were exposed to a step increase of 1000 µg/mL spectinomycin at time zero. Without the resistance provided by MexXY, all Δ*mexY* cells quickly stopped growing following drug exposure.

Supplementary Video 5 - WT cells exposed to 700 µg/mL spectinomycin show reduced growth. WT cells carrying the native *mexXY* resistance mechanism and a MexY reporter plasmid were exposed to a step increase of 700 µg/mL spectinomycin at time zero. WT cells mostly show reduced growth but survive this drug concentration, unlike the heterogeneous cell fates of WT cells exposed to 1000 µg/mL spectinomycin.